Rapid glaciation and a two-step sea-level plunge into The Last Glacial Maximum

Citation for published version:
Yokoyama, Y, Esat, TM, Thompson, WG, Thomas, A, Webster, JM, Miyairi, Y, Sawada, C, Aze, T, Matsuzaki, H, Okuno, J, fallon, S, Braga, JC, Humblet, M, Iryu, Y, Potts, D, Fujita, K, Suzuki, A & kan, H 2018, 'Rapid glaciation and a two-step sea-level plunge into The Last Glacial Maximum' Nature. DOI: 10.1038/s41586-018-0335-4

Digital Object Identifier (DOI):
10.1038/s41586-018-0335-4

Link:
Link to publication record in Edinburgh Research Explorer

Document Version:
Peer reviewed version

Published In:
Nature

Rapid glaciation and a two-step sea-level plunge into The Last Glacial Maximum

Yusuke Yokoyama[1, 2, 3]*, Tezer M Esat[4,5], William G Thompson[6], Alexander L Thomas[7], Jody M. Webster[8], Yosuke Miyairi[1], Chikako Sawada[1], Takahiro Aze[1] Hiroyuki Matsuzaki[9], Jun'ichi Okuno[10], Stewart Fallon[4], Juan-Carlos Braga[11], Marc Humblet[12], Yasufumi Iryu[13], Donald C Potts[14], Kazuhiko Fujita[15], Atsushi Suzuki[16], Hironobu Kan[17]

[1.] Atmosphere and Ocean Research Institute, University of Tokyo, Japan. [2.] Department of Earth and Planetary Science, Graduate School of Science, University of Tokyo, Japan. [3.] Japan Agency for Marine-Earth Science and Technology, Yokosuka, Japan. [4.] Research School of Earth Sciences, Australian National University, Canberra, ACT, Australia. [5.]Research School of Physics and Engineering, Australian National University, Canberra, ACT, Australia. [6.] Woods Hole Oceanographic Institution, Woods Hole, MA, United States. [7.] University of Edinburgh, Edinburgh, United Kingdom. [8.] University of Sydney, Sydney, NSW, Australia. [9.] University Museum, University of Tokyo, Japan. [10.] National Institute of Polar Research, Japan. [11.] Universidad de Granada, Granada, Spain. [12.] Nagoya University, Nagoya, Japan. [13.] Tohoku University, Sendai, Japan. [14.] University of California Santa Cruz, Santa Cruz, CA, United States. [15.] University of Ryukyu, Japan. [16.] Geological Survey of Japan, Japan [17.] Kyushu University, Japan.

The ~10 kyr-long Last Glacial Maximum (LGM), prior to the termination of the last ice age, was the coldest period in Earth's recent climate history[1]. Relative to the Holocene, atmospheric CO_2 was about 100 ppm lower and tropical sea surface temperatures were about 3-5 °C colder[2,3]. The LGM began when global mean sea level (GMSL) abruptly dropped by ~40 m at ~31 kyr ago[4] and was followed by ~10 kyr of rapid deglaciation into the Holocene[1]. The masses of the melting polar ice sheets, the change in ocean volume and hence GMSL are primary constraints for climate models constructed to describe the LGM-Holocene transition and future changes, but important facets of the transition – including the rates, timing, and magnitude – remain enigmatic. Here we show that sea level at the shelf edge of the Great Barrier Reef (GBR) dropped by ~20 m from 22-21.5 ka, to -118 m below modern. Our findings are based on recovered and radiometrically-dated fossil corals and coralline algae assemblages, and represent relative sea level (RSL) at the GBR, rather than GMSL. Subsequently, RSL rose at a rate of ~3.5 mm/yr for ~4 ky. The rise is consistent with the warming previously observed at 19 kyr ago[1,5], but we now show it occurring just after the 20 m RSL drop and related increase in global ice volumes. The

detailed structure of our new record is robust as the GBR is remote from former ice sheets and tectonic activity. RSL can be influenced by the Earth's response to regional changes in ice and water loadings and may significantly differ from GMSL. Consequently, we used glacio-isostatic (GIA) models to derive GMSL, and find that the LGM culminated in a GMSL low of about -125 to -130 m.

The LGM to Holocene sea level rise was at times episodic and stimulated particular patterns in coral reef growth and evolution. Estimates of the maximum volume of excess ice and amount of water that contributed to the change in the corresponding GMSL was originally based on the stratigraphy of radiocarbon and U-series dated corals from Barbados[6,7]. Data from radiocarbon dated micro and macro fossils also helped define LGM paleo-shorelines from Sunda Shelf in South China Sea[8] and Bonaparte Gulf of Northern Australia[5,9]. However, large uncertainties remain in local relative sea level data and in GIA model inputs, such as ice histories and Earth rheology. These are needed in estimating the bounds of past and future global mean sea levels which, for the LGM, range from 115 m to 135 m[4,10].

Precise and accurate sea level histories, often derived from dating of fossil corals and algae, are important. Coastal shelf geometry and location of land-bridges and islands at the LGM have a bearing on probable human migration routes and impact the ecological and species diversity, for example, of endemic flowering plants on islands that had complex, dynamic histories and covered a larger area during the LGM[11]. Sea-levels vary with polar ice volumes and the extent of LGM ice-sheets can affect atmospheric pressure patterns and alter the salinity of oceans causing circulation changes[4].

Fossil coral and coralline algae deposits of the LGM-Holocene period at the GBR are below present sea level and were drilled during the Integrated Ocean Drilling Program (IODP) Expedition 325 in 2010[12] (Fig.1). Corals and coralline algae were recovered from 34 holes, over two transects 500 km apart, at Hydrographers Passage (HYD-01C) and Noggin Pass (NOG-01B; Fig.1). Depths, up to 150 m below sea level were reached to access the full LGM period[12]. Selected, well characterized, samples were dated by U-series (coral) and accelerator based radiocarbon (coral and algae) methods (Extended Data Table 1). Sea level depth uncertainties depend on the paleo-habitat depth range of particular coral and algae species and were conservatively assessed in conjunction with associated algal crust thickness, vermetid gastropods and by benthic foraminiferal assemblages[12,13] (Figs. 2, 3; Methods; Extended Data Figures 1-6).

A brief outline of previous determinations of the timing and duration of the LGM shows it extended from about 29.5 to 19 ka[1]. There is an initial rapid (>40 m) fall in GMSL from 31-32 ka to 29-30 ka (Fig. 4a, 4b) [1,4]. A protracted gradual GMSL drop was construed from about 29 ka to 21 ka[4]. However, this was largely an extrapolation between the two endpoints due to the sparsity of data which also have large (~20 m) uncertainties in RSL elevations (Fig 4c, 4e) [4,5,6,7]. Onset of deglaciation is apparent from 21 ka with a gradual 10-15 m GMSL rise[4] followed by a short stable or possibly slowly falling GMSL from ~18 ka to ~16.5 ka (see Figs. 4a, 4b of Ref. 4). From here on, the deglaciation proceeded at a fast pace, at times, exceeding ~12 m/ky during the so-called meltwater pulses[14,15].

We have converted our new GBR local sea levels to global values through GIA modelling (methods) which accounts for the higher GBR coastline elevations due to increased ice volumes and reduced adjacent ocean water loading. The present results significantly diverge from earlier determinations and completely revise the internal structure of the LGM GMSL (Fig. 4b). A large number of data points from Noggin and Hydrographers sections show a relatively constant sea level from about 28 ka to 22 ka after the initial rapid fall from 31 ka[4] as documented previously from Barbados, Huon and Bonaparte Gulf (Figs. 3, 4c-4h). The GMSL remains invariant from 30 ka to 21.5 ka at mean value of 113 m within a range of about ±6 m and represents the early LGM period, LGM-a (Fig. 4b; red band). This is significantly shallower than former estimates[4] (Fig. 4b). The previously identified[16,17] ~19ka, “onset-of-degraciation”, in fact, corresponds to a rapid sea level fall followed by a ~4,000 year-long ~3.5 m/kyr sea level rise. We label this period as LGM-b, lasting from about 21 ka to 17 ka. The minimum GMSL at LGM-b ranges from about 130 m to 125 m due to analytical uncertainties and uncertainties in Earth model parameters and occurs after a ~20 m drop (Methods, Extended Data Fig. 8,9 and Table 1). This point defines the start of LGM-b, after which the GMSL slowly rises to 120 m at about 17 ka followed by a rapid transition towards full deglaciation. The rate of net ice mass gain or sea-level fall at the inception of both the LGM-a (~30 ka) and LGM-b (~21 ka) are similar and range approximately from 15 to 20 mm per year as determined from the slopes of the GMSL curves. This GIA modelled, very fast, maximum glaciation rate is significantly faster than the mean LGM-Holocene deglaciation rate of ~12 mm/year[4]. The sea-level drop at LGM-b is strikingly evident in cores from both HYD and NOG sections as a major growth hiatus in cores M0031-33A and M0055A 33 (Fig. 2). Deposits of fresh water calcite cement, in corals below the hiatus, indicate subaerial exposure and low sea levels (Methods; Extended

Data Figure 5). In turn, the gap corresponding to the sea-level low is picked up at five other sites, M0035, 36, 39, 53 and 54, at lower elevation, to complete the sea-level curve (Extended Data Fig. 3).

We have established an ice model, based on the new GBR RSL data that provides a good agreement with other far-field RSL records when combined with a range of Earth model parameters that span the possible range of viscosities for the upper and lower mantle as well as lithospheric thickness. Model predictions of RSL's, over the LGM-a and -b periods, generally agree well with the trends derived from existing data (Fig. 4, Extended Data Figure7; Supplementary Information). The magnitude of the sea level drop at the start of the LGM[1,4] (≈29 ka) is about 40 m, constrained by coral data from Huon Peninsula[18] and Barbados [19] and with foraminifera oxygen isotope records from the Red Sea[20] within relatively large (ca.10 m) uncertainties. There is also close agreement between model results and data over the deglaciation period from 17 ka onwards except at Barbados (Fig. 4c). Here, the systematic overshoot of the data above the sea level curve is indicative of additional processes, possibly, of tectonic nature[15]. This is consistent with independent evaluations including the study[10] using the rate of change of degree-two harmonics of Earth's geopotential due to GIA.

The very rapid build-up of global ice volume during the two periods of transition at LGM-a (~29-31 ka; Ref 4, Fig. 4D) and LGM-b (~22-21 ka; Fig. 4b, present work) requires substantial moisture transport and snow precipitation over existing ice sheets. To accommodate LGM-b an additional equivalent ice volume corresponding up to 17 m of sea level is required. The location of the extra ice cannot be determined with certainty. GIA modelling and Northern and Southern Hemisphere (NH, SH) bipolar climate paced by complementary high latitude insolation highs [1,21,22] at these times shows increased ice volume over the North American Ice Sheet (NAIS) at LGM whereas the Eurasian ice sheet appears to have grown at a slower pace and commenced melting after ≈22 ka (Extended Data Fig. 8). Colder Antarctic climate during the LGM[3,16] is likely to have hindered ice calving and lessened basal melting of ice shelves resulting in increased ice volume. The sustained growth of the AIS during the LGM-b period and beyond, including continuing ice accumulation up to around 14 ka, agrees with observations of the late retreat of West Antarctic Ice Sheet at this time [1,23,24]. However, the major increase in ice volume, precipitating the onset of LGM-b, appears to have been during a short period (20 ka to 21 ka) over the NAIS after which the NAIS retreated from ≈20 ka onwards[25] (Extended Data Fig. 8).

The enlarged global ice volume at ~30 ka[1,4,18,26], equivalent to ~40 m of sea-level drop, persisted for over ~8 thousand years. Similarly, the low NH insolation and somewhat reduced atmospheric CO_2 levels around ~21 ka to ~22 ka led to a period of cold climate, very low tropical Atlantic SST's and ultimately the transition to LGM-b. At this time, increased SH insolation is likely to have facilitated moisture transport to the South, increasing the AIS volume[1,18,27]. Heinrich event 1 at ~17 ka marks the end of LGM-b when full deglaciation kicked-in as the pace of NH insolation and atmospheric CO_2 levels increased rapidly (Fig. 4).

The two sharp transitions preceding LGM-a and LGM-b periods, associated with rapid accumulation of ice and lower sea levels, at the end of the last ice age, do not appear to be explicable in terms of processes attributable to any specific climate-change dynamic. During this time (~29-19 ka), oxygen isotope records in ice cores do not show a clear, distinct signal; the CO_2 levels were stable, insolation at the time was not so different to present and tropical SST did not change significantly[1,28]. A systematic behaviour in sea level and climate has previously been noted[29] whereby transitions between two states, cold to warm or warm to cold, took place through a third more extreme state as in MIS3-LGM-Holocene or during the Last Interglacial (LIG), LIG-(LIG high-stand at the end of LIG)-(MIS 5d). A similar behaviour in climate was previously noted where the appearance of an intermediate, extreme third state, may have resulted in a shift from “41-ky” cycles to “100-ky” cycles 800 ka to 1 Ma ago[30]. These bifurcations can be thought of as states in three climate potentials with “stochastic climate noise” causing transitions between them[30]. Here, it appears that the same behaviour may occur over short timescales, not only over 100 ka cycles. The transitions are not only manifest in climate but are also associated with sea-level change.

References:

1. Clark, P. U., Dyke, A.S., Shakun, J.D., Carlson, A.E., Clark, J., Wohlfarth, B., Mitrovica, J.X., Hostetler, S.W., and McCabe, A.M. The Last Glacial Maximum. *Science* **325**, 710-714 (2009).

2. Felis, T., McGregor, H. V., Linsley, B. K., Tudhope, A. W., Gagan, M. K., Suzuki, A., Inoue, M., Thomas, A. L., Esat, T. M., Thompson, W. G., Tiwari, M., Potts, D. C., Mudelsee, M., Yokoyama, Y., Webster, J. M.,. Intensification of the meridional temperature gradient in the Great Barrier Reef following the Last Glacial Maximum. *Nature Communications* **5**, 4102, doi:10.1038/ncomms5102 (2014).

3. Mix, A. C., E. Bard, and R. Schneider. Environmental processes of the ice age: land, oceans, glaciers (EPILOG). *Quaternary Science Reviews* **20**, 627-657 (2001).

4. Lambeck, K., Rouby, H., Purcell, A., Sun, Y., Sambridge, M. Sea level and global ice volumes from the Last Glacial Maximum to the Holocene. *Proceedings of National Academy of Science of the United States of America* **111**, 15296-15303, doi:10.1073/pnas.1411762111 (2014).

5. Yokoyama, Y., Lambeck, K., DeDeckker, P., Johnston, P., and Fifield, L.K. Timing of the Last Glacial Maximum from observed sea-level minima. . *Nature* **406**, 713-716 (2000).

6. Fairbanks, R. G., A 17,000-year glacio-eustatic sea level record: influence of glacial melting dates on Younger Dryas event and deep ocean circulation. *Nature* **342**, 637-642 (1989).

7. Bard, E., B. Hamelin, and R.G. Fairbanks. U-Th ages obtained by mass spectrometry in corals from Barbados: sea level during the past 130,000 years. *Nature* **346**, 456-458 (1990).

8. Hanebuth, T., K. Stattegger, and P.M. Grootes. Rapid flooding of the Sunda Shelf: a late-glacial sea-level record. *Science* **288**, 1033-1035 (2000).

9. DeDeckker, P., and Y. Yokoyama. Micropalaeontological evidence for Late Quaternary sea-level changes in Bonaparte Gulf, Australia,. *Global and Planetary Change* **66**, 85-92 (2009).

10. Nakada, M., Okuno, J.,and Yokoyama, Y. Total meltwater volume since the Last Glacial Maximum and viscosity structure of Earth's mantle inferred from relative sea level changes at Barbados and Bonaparte Gulf and GIA-induced J2. *Geophysical Journal International* **204**, 1237-1253, doi:10.1093/gji/ggv520 (2016).

11. Weigelt, P., Steinbauer, M. J., Cabral, J. S. & Kreft, H. Late Quaternary climate change shapes island biodiversity. *Nature*, doi:10.1038/nature17443 (2016).

12. Webster, J. M., Braga, J.C., Humblet, M., Potts, D.C., Iryu, Y., Yokoyama, Y., Fujita, K., Bourillot, R., Esat, T.M., Fallon, S., Thompson, W.G., Thomas, A.L., Kan, H., McGregor, H.V., and Hinestrosa, G. Response of the Great Barrier Reef to sea level and environmental changes over the past 30 ka. *Nature Geoscience* **accepted** (2017).

13. Yokoyama, Y., and T.M. Esat. in *Handbook of Sea-Level Research* (ed I. Shennan, Long, A., and Horton, B.) Ch. 7, 104-124 (John Wiley & Sons, 2015).

14. Deschamps, P., N. Durand, E. Bard, B. Hamelin, G. Camoin, A.L. Thomas, G.M. Henderson, Okuno, J., and Y. Yokoyama. Ice-sheet collapse and sea-level rise at the Bølling warming 14,600 years ago. *Natrue* **483**, 559-564 (2012).

15. Bard, E., B. Hamelin, and Delanghe-Sabatier, D. Deglacial Meltwater Pulse 1B and Younger Dryas Sea Levels Revisited with Boreholes at Tathiti. *Nature* **327**, 1235-1237 (2010).

16. Clark, P. U., A.M.McCabe, A.C.Mix, and A. J. Weaver. Rapid rise of sea level 19,000 years ago and its global implications. *Science* **304**, 1141-1144 (2004).

17. MARGOProjectMembers. Constraints on the magnitude and patterns of ocean cooling at the Last Glacial Maximum. *Nature Geoscience* **2**, 127-132 (2009).

18. Cutler, K. B., R.L. Edwards, F.W. Taylor, H. Cheng, J. Adkins, C.D. Gallup, P. M. Cutler, G.S.Burr, and A.L. Bloom. Rapid sea-level fall and deep ocean temperature change since the last interglacial period. *Earth and Planetary Science Letters* **206**, 253-271 (2003).

19. Peltier, W. R., and Fairbanks, R.G. Global glacial ice volume and Last Glacial Maximum duration from an extended Barbados sea level record. *Quaternary Science Reviews* **25**, 3322-3337 (2006).

20. Grant, K. M., E. J. Rohling, M. Bar-Matthews, A. Ayalon, M. Medina-Elizalde, C. Bronk Ramsey, C. Satow and A.P. Roberts. Rapid coupling between ice volume and polar temperature over the past 150,000 years. *Nature* **491**, 744-747 (2012).

21. Abe-Ouchi, A. *et al.* Insolation-driven 100,000-year glacial cycles and hysteresis of ice-sheet volume. *Nature* **500**, 190-193, doi:10.1038/nature12374 (2013).

22. Pilippon, G., G. Ramstein, S. Charbit, M. Kageyama, C. Ritz, and C. Dumas. Evolution of Antarctic ice sheet throughout the last deglaciation: A study with a new coupled climate- north and south hemisphere ice sheet model. *Earth and Planetary Science Letters* **248**, 750-758.

23. Anderson, J. B. *et al.* Ross Sea paleo-ice sheet drainage and deglacial history during and since the LGM. *Quaternary Science Reviews* **100**, 31-54, doi:10.1016/j.quascirev.2013.08.020 (2014).

24. Yokoyama, Y., Anderson, J.B., Yamane, M., Simkins, L.M., Miyairi, Y., Yamazaki, T., Koizumi, M., Suga, H., Kusahara, K., Prothro, L., Hasumi, H., Southon, J.R., and Ohkouchi, N. Widespread collapse of the Ross Ice Shelf during the late Holocene. *Proceedings of National Academy of Science of United States of America* **113**, 2354-2359 (2016).

25. Lambeck, K., Purcell, A. & Zhao, S. The North American Late Wisconsin ice sheet and mantle viscosity from glacial rebound analyses. *Quaternary Science Reviews* **158**, 172-210, doi:10.1016/j.quascirev.2016.11.033 (2017).

26. Clark, P. U. & Tarasov, L. Closing the sea level budget at the Last Glacial Maximum. *Proc Natl Acad Sci U S A* **111**, 15861-15862, doi:10.1073/pnas.1418970111 (2014).

27. Clark, P. U., Hostetler, S.W., Pisias, N.G., Schmittner, A., and Meissner, K.J. Mechanisms for a ~7-kyr climate and sea-level oscillation during marine isotope stage 3. *Ocean Circulation: Mechanisms and Impacts* American Geophysical Union, Geophysical Monograph 173, pp. 209-246. (2007).

28. Brook, E. J. *et al.* Timing of millennial-scale climate change at Siple Dome, West Antarctica, during the last glacial period. *Quaternary Science Reviews* **24**, 1333-1343, doi:10.1016/j.quascirev.2005.02.002 (2005).

29. Yokoyama, Y., and T.M. Esat. Global Climate and Sea Level-Enduring variability and rapid fluctuations over the past 150,000 years. *OCEANOGRAPHY* **24**, 54-69 (2011).

30. Paillard, D. Quaternary glaciations: from observations to theories. *Quaternary Science Reviews* **107**, 11-24, doi:10.1016/j.quascirev.2014.10.002 (2015).

Supplementary Information is available in the online version of the paper.

Acknowledgements We thank the IODP and ECORD (European Consortium for Ocean Research Drilling) for drilling the GBR, and the Bremen Core Repository for organizing the onshore sampling party. Financial support of this research was provided by the JSPS KAKENHI (JP26247085, JP15KK0151, JP16H06309, JP17H01168), Australian Research Council (grant DP1094001), ANZIC, NERC grant NE/H014136/1 and Institut Polytechnique de Bordeaux. This paper is a contribution to INQUA commission on Coastal and Marine Processes and PAGES PALSEA2 program.

Author Contributions Y.Y. and J.M.W. were co-chief scientists of Expedition 325. J.O. and Y.Y. conducted GIA modeling. Y.Y. and T.M.E. wrote the manuscript in collaboration with J.M.W., A.L.T., J.C.B, M.H., and the paper was refined by contributions from the rest of the co-authors.

Competing interest The authors declare no competing interests.

Author Information Correspondence and requests for materials should be addressed to Y.Y. (yokoyama@aori.u-tokyo.ac.jp).

Figure Legends

Figure 1

Location of GBR Expedition 325 study site. The Northern and Southern sites are at Cairns (Noggin Pass – NOG01B) and at Mackay (Hydrographer's Passage – HYD-01C). High-resolution 3D multibeam image showing the surface geomorphic context[12], drill transects and specific locations of the drill holes.

Figure 2

Last Glacial Maximum sea level drop at LGM-b. Here, captured clearly as a distinct age discontinuity observed in cores M0055A and M0031-33A from NOG and HYD transects respectively, separated by more than 500 km in the GBR. Cores obtained from different fossil GBR terraces and reefs reveal the trajectory of past sea level changes. Five reef sequences are distinguished based on the IODP Exp. 325 record: Reef 1 (≥ 30 ka), Reef 2 (27-22 ka), Reef 3 (3a, 21-17 ka; 3b, 17-13 ka), Reef 4 (13-10 ka), and Reef 5 (modern GBR). The major growth hiatus evident from both HYD and NOG sections marks the death of Reef 2 (22.1 ka to 21.9 ka) following the sea level fall leading to LGM-b and reestablishment of reef (Reef 3a) further seaward at 20.7-20.5 ka (Extended Data Figs. 3, 4, 5). The age versus depth relationships, and the presence of fresh water low magnesium calcite cement, in Reef 2, confirms subaerial exposure during the LGM-b period. In contrast, their absence below Reef 3a deposits places a maximum limit on the sea level fall (Methods). At the end of LGM, after 17 ka, sea level rose rapidly flooding the outer shelf causing the re-establishment of the reef over its former position (Reef 3b), marking the end of hiatus at the top of Reef 2 at ~17 ka. The details of the transition to LGM-b and the critical samples defining the fall in sea-level are shown in Extended Data Fig. 6.

Figure 3

Age versus depth plots showing the RSL envelopes derived from samples recovered by IODP Expedition 325. Both HYD (panel a, blue) and NOG (panel b, red) transect cores were examined for coral, coralgal algae and benthic foraminiferal assemblages (Extended Data Figs. 1, 2) with help of X-ray CT scan and X-ray diffraction (Supplementary Information) that revealed detailed features of relative sea level histories during the past 35,000 years. The >500 dates, selected through detailed sedimentologic and biologic analyses (Methods), provided a robust chronostratigraphic framework that defined five distinct reef sequences (Reefs 2 to 4 are labeled on Fig. 2) which grew episodically over the past 30 ka. The RSL's constructed here depend on the age (horizontal grey line) and sea level depth uncertainties (upward and downward grey lines) related to paleo-habitat depth range (upward line) of each dated coral or algal sample and the maximum coring depth uncertainty (downward line). The paleowater depth ranges for shallow water species (blue and red envelopes) were conservatively estimated using a multiproxy approach combining coral, coralline algae and other key indicators such as algal crust thickness, and the presence of vermetid gastropods (Methods, Extended Data Table 1). Note the disconnected paleowater depth lines on some samples are indicative of deeper habitat ranges likely > 20 m water depth. The distribution of marine and fresh water cements in the cores were used to support the new estimates of the timing and magnitude of the LGM-b sea levels (Extended Data Figs. 3-5), including hiatuses and regressions.

Figure 4

Global mean sea levels (GMSL) and GIA model derived far-field RSL with observational data. Previously constructed global mean sea level curve over the past 140 ka[4], blue line in panels a, b, is shown together with GIA model predictions, in panels c-h, for selected far-field data represented by red circles with depth and age error bars. High latitude (65 °) summer insolation curves for Northern and Southern Hemispheres in panel (b) are shown as dashed orange and blue lines respectively. Long term sea level variation is in step with Northern Hemisphere summer insolation whereas LGM-b occurs at the peak of Southern Hemisphere insolation. Orange circles in each panel (c-h) indicate previously reported RSL with depth and age uncertainties (horizontal and vertical black lines). Results of 62 GIA model runs (Methods), over a range of potential earth model parameters, such as lithospheric thickness and viscosities of both upper and lower mantle, are within the orange (a-b) and gray bands in (c-h). The red and blue curves in grey shaded bands (c-h) show the results for lower mantle viscosities of 10^{22} and 10^{23} Pa s respectively with 70 km lithospheric thickness and upper mantle viscosity of 10^{20} Pa s. Of note is the foraminiferal oxygen isotope based Red Sea data[20] (h) which supports the new GMSL calculations from the present study within uncertainties (ca. 10 m). The orange band in (h) is confidence intervals of 95% for the RSL data (light orange) and probability maximum (dark orange) reported in ref. 20.

Methods

IODP Expedition 325: The Great Barrier Reef environmental changes.

The Integrated Ocean Drilling Program (IODP) Expedition 325 was designed to complement the previous IODP “Tahiti Sea Level” Expedition 310 to Tahiti[31]. In preparation for Expedition 325, potential drill sites were surveyed with the CSIRO ship *RV Southern Surveyor* using multibeam sonar, seismics, an AUV and rock dredging[12,32]. At most of the Great Barrier Reef (GBR) locations, the shelf breaks at approximately 120 m and is populated with prominent terrace-like structures and other relict reefs appear successively at 100-90 m, 60-50 m and 35-40 m depths[33-35].

The mission specific platform chosen for Expedition 325 was the *Greatship Maya,* an IMO class II vessel capable of being positioned dynamically for *geotechnical* coring[32,35]. The expedition took place between 12 February and 6 April 2010. A total of 34 holes across 17 sites were sampled ranging in depth from 46.4 m to 170.3 m such that the recovered coralgal deposits span several crucial but poorly defined periods during the LGM and last deglaciation. Sampling occurred at three locations along the North Eastern coast of Australia but this study focuses on one transect at 19.7° latitude offshore from Cairns at Noggin Pass (NOG-01B), and another at 17.1° latitude, offshore Mackay at Hydrographer’s Passage (Fig. 1, HYD-01C). Photographs of half-sectioned reef cores, relevant to the present study, are shown in (Extended Data, Figs. 1, 2) together with the depths and genera of the dated corals and coralline algae. Classification of coral genera and species in terms of their habitat preferences according to depth and turbulence levels is also supported by considering the habitats of associated coralline algae taxa and crust thickness and vermetid gastropods. For example, individual coralline algae can have limited range of habitats bounded by sensitivity to light levels, wave energy and other factors and can be used to more accurately constrain the paleo-depth ranges. Based on this careful and detailed multi-proxy approach each dated coral and coralline algae sample was placed within an internally consistent coralgal assemblage and paleobathymetric scheme[36,37] enabling the construction of an independent RSL envelope at each site (Extended Data Figs. 1, 2, 3,Table 1 and Supplementary Information).

Main lithologic facies observed in the Expedition 325 cores.

The main lithologies are divided into coral reef framework and detrital sedimentary facies. The three boundstone facies are defined by their varying proportions of corals, coralline algae and microbial deposits forming coralgal, coralgal-microbialite and microbialite-dominated boundstones. The detrital facies can occur locally as internal sediments within the boundstones, or as metre scale intervals of packstones to rudstones and unconsolidated sediments. Details of facies and depth estimate using facies as well as coral and coralline algae assembly can be found in Extended Data Figures 1 and 2 and Table 1, and are derived from Webster et al.[12].

Reef 2 hiatus and GMSL drop to LGM-b

A major growth hiatus is observed in the inner shelf terrace at 104-106 mbsl, at both HYD-01C M0031-33A) and NOG-01B (Hole M0055A) (Extended Data Figs. 3 and 4) [12]. This represents the turn-off of Reef 2 at ~ 21 ka and is interpreted to be caused by the drop in sea-level to the LGM-b. The coralgal assemblages show that paleowater depths were shallow (<10 m) just prior to Reef 2 death, and lithologic, and seismic evidence indicates this was a major subaerial exposure surface[12]. Furthermore, detailed scanning electron microscopic (SEM), energy-dispersive X-ray spectrum (SEM-EDS), X-ray diffraction (XRD) analyses and thin-section observations of Reef 2 deposits confirm that they were exposed to freshwater or subaerial environments (e.g. low magnesium calcite cements in Hole 55A Core 4R1) during the sea level lowstand at LGM-b (Extended Data Fig 5). At this time shallow reef development migrated ~1 to 0.25 km seaward (ie. Reef 3a) in <2 kyr, as the RSL sea level fell to 118 m below present by ~20.5 ka. The Reef 3a deposits and the older > MIS3 deposits are characterized by wholly marine diagenetic features consistent with the interpretation that the LGM-b sea level did not fall below this level (Extended Data Fig 6). Sea level rose during the deglacial causing major Reef 3a aggradation[12] before re-flooding the inner shelf terraces at ~ 16.5 ka and causing the re-establishment of the reef (Reef 3b) over its former position, marking the end of the hiatus at the top of Reef 2.

Determining the ages of sea level indicators

Representative, more than 165, coral skeletons and their aragonite content were analyzed by powder X-ray diffraction, X-radiography, SEM and petrologic investigations, all of which confirmed to the pristine nature of the dated samples[2]. In a few cases, X-ray diffraction picked up minor signatures of Hi-Mg calcite, likely due to trace amounts of coralline algae and microbialite sediment. Yet no significant calcite peaks were observed in most of the cases. Physical cleaning of branched corals for U-Th dating and severe acid dissolution of samples, namely more than 50% of the weight, for radiocarbon dating was used to remove potential secondary precipitated materials. For massive *Porites* corals, physical cleaning is difficult requiring further geochemical tests including ICP-MS. Skeletal Mg/Ca ratios confirmed the absence of significant amounts of high-Mg calcite and secondary aragonite cements. Even the case when the secondary aragonite was found, the ages are not affected significantly since the form of the cements are indicative of early phase of post mortem of corals. Further evaluations included limits on total uranium, ^{232}Th content and initial ^{234}U/^{238}U ratio. We applied different initial ^{234}U/^{238}U criteria: for samples of the deglacial period between 17 ka and 0 ka, the acceptable range was 1.1452 +/- 0.0140, whereas for the samples from 30 ka to 17 ka 1.1402 +/-0.0140 was used. All of data used to reconstruct the relative sea level envelopes for each transect are shown in Supplementary Information (see Methods Section *Relative Sea level (RSL) reconstruction* for more details) and the primary samples used to determine the specific RSL inflection points are indicated as "HY-1, 2.." and "NO-1, 2.." for HYD-01C and NOG-01B respectively in the Supplementary Information and highlighted in bold. U-series and radiocarbon ages from the same coral samples also showed remarkable consistency, along with radiocarbon ages on directly adjacent coralline algae. Taken together, and combined with the consistent reproducibility of the relative sea level envelopes between two transects, more than 500 km apart, confirms the veracity of the data.

Radiocarbon dating

More than 500 radiocarbon dates were obtained using corals and coralline algae samples which were all processed at the Atmosphere and Ocean Research Institute (AORI), the University of Tokyo (UTokyo) to convert them into graphite[38]. Typically 1mg or more of graphite was measured using a Single Stage Accelerator Mass Spectrometry at AORI[39] and at the Australian National University (ANU; [40]). The results were then converted to calendar ages with local reservoir ages (12±10 years) from[41], which we obtained by averaging between Heron Island (8±6 years) and Abraham Reef values (15±6 years). The calibration was then performed using international calibration datasets (IntCal 13 and Marine 13;[42])

Analytical procedures, Mass spectrometry and U-Th dating.

The analytical data are listed in Supplementary Information. Consistency between labs for replicate measurements of a single specimen is within 100 years, which is similar to the intra coral variability observed in some specimens measured using the high precision (WHOI) method. Uranium series dating were conducted at three different labs: the Australian National University (ANU), the University of Oxford (OX) and the Woods Hole Oceanographic Institute (WHOI). A 61-cm mass spectrometer is used at ANU, which can operate in charge-mode[43]. The $^{229-230-232}$Th isotopes were measured simultaneously in charge-mode in Faraday cups using 20pF feed-back capacitors as active electrometer elements. Uranium isotopes, $^{233-234-235}$U were also measured in charge-mode, whereas ^{238}U was simultaneously measured using a 10^{10} Ohm feed-back resistor. The magnitude of the ^{238}U low-mass tail was monitored continuously at mass ^{237}U in charge mode. This was used to subtract the ^{238}U tail from under the $^{233-234-235}$U isotopes. Extensive measurements with an un-spiked U-standard HU-1 showed that the shape of the ^{238}U tail remained invariant under a wide range of conditions, in particular, at the expected locations of the $^{233-236}$U peaks. Sample loads, on single rhenium filaments, ranged from 0.5 to 0.8 μg and the ^{238}U beam intensity was kept between $8x10^{11}$ to $10x10^{11}$ Ampere for several hours. At these intensities, 10^{10} Ohm feedback resistor was used to avoid response-time problems encountered with the considerably slower 10^{11} Ohm resistors. The instrument was calibrated with reference to a secular-equilibrium standard HU-1.Comparisons with Western Australian last interglacial samples[44] and with Hulu-Cave speleothem data[45] showed precise agreement with previous measurements. Sample processing followed previously established procedures[46]. U and Th were separated from the coral carbonate using U-Teva resin in a single pass.

Uranium thorium dating at OX and WHOI were measured by multi-collectors ICP-MS. At OX, U and Th isotopes were measured with ion counter collectors for the minor isotope beams. Approximately 0.3g of coral sample was dissolved and spiked with a mixed $^{236}U:^{229}Th$ tracer. U and Th were purified and measured separately: U isotopes, statically; and Th by peak hopping the 229 and 230 beams into an ion counter while normalizing beam intensity between the steps with either ^{232}Th or ^{235}U measured in Faraday collectors. Instrumental biases and relative collector efficiencies are accounted for using standard sample bracketing using U and Th isotope standards[47].

At WHOI U and Th isotopes were measured by MC-ICP-MS in static mode with all isotopes in Faraday collectors[48]. Large ~5g subsamples of coral were dissolved and spiked with a mixed $^{233}U:^{236}U:^{229}Th$ tracer, optimised for the last glacial maximum to deglacial age samples, and co-precipitated with Fe. To determine the $^{230}Th/^{238}U$, purified U and Th fractions are recombined such that U and Th are measured together at isotope ratios that can be closely matched to bracketing standards. The $^{234}U/^{238}U$ is similarly determined statistically in Faraday collectors but on an unspiked aliquot.

All activity ratios and ages are calculated using the half-lives reported in[45]. Ages are presented in Extended Data Table 1 as ‘raw’, assuming all ^{230}Th is accumulated in the coral since growth, and an age corrected for detrital ^{230}Th. The detrital correction makes use of the measured $^{232}Th/^{238}U$ as a proxy for the amount of detrital contamination, an assumed detrital composition of crustal origin[49], and an allowance for non-secular equilibrium of the contaminant.

Relative sea level (RSL) reconstruction

The sample context was assessed using established criteria[12,32] including: (1) core quality, (2) orientation of well-preserved corallites; (3) thick coralline algal crusts capping upper coral surfaces; (4) evidence of substrate attachment; and (5) the presence/absence and orientation of geopetals in lithified facies . Based on these criteria all the samples were classified into the following four context categories: (1) IS = in situ (convincing supporting evidence), (2) IS? = likely insitu (inclusive supporting evidence), (3) ISX = not in situ (convincing nonsupporting evidence, and (4) ISN = status not known (inadequate evidence either way). Samples from highly drill-disturbed or poor recovery intervals were excluded. A total of 540 samples satisfying these criteria were used to construct a RSL envelope (upper and lower bounds) at both sites. Despite known temporal differences in ocean reservoir age, the coral U/Th and coral/coralline ^{14}C AMS ages are remarkably consistent. However, wherever possible we used the more precise U/Th coral ages to constrain the upper and lower bounds of the envelopes. This was achieved by visually fitting a line through the dates that were >1 m apart and outside their analytical age errors, while also taking into account the upper bound of the paleowater depth estimate of each sample and any core recovery uncertainties (Supplementary Information). Where multiple coral dates overlapped (in time) we used the mid-point between samples. If replicate age determinations were available for the same sample (ie. same coral colony or coralline algal crust) (Supplementary Information) an average age was calculated and plotted on Fig. 3. The upper bound or minimum position of the sea level envelope was further constrained by considering the overlapping paleowater depth ranges of both the shallow water sea level indicators and their coeval, deeper forereef slope equivalents. Finally, the major inflection points marking clear changes in the direction, amplitude and rate of RSL change were also identified each envelope (Fig. 3). Thus the lower bound (i.e. maximum sea level position) of RSL curves and the specific samples defining them are indicated in bold in Supplementary Information (ie. HY-1, 2.., NO-1, 2..) and a close up of the key samples constraining LGM-b is also shown in Extended Data Figure 6.

GIA model predictions

The GIA model calculations included an earth model describing the viscoelastic properties of the solid earth, as well as an ice component documenting the ice melting history, reconstructed mainly from far-field sea-level observations[4,50]. The Earth model is based on seismologically derived "Preliminary Reference Earth Model" (PREM) [51] and consisted of an elastic lithosphere with an upper and lower mantle divide at 670 km depth. The lithosphere thickness was 70km and upper and lower mantle viscosities ranged from (1-10) x 10^{20} Pas and (1-100) x10^{22} Pas respectively. This model provides an accurate treatment of time-dependent continental shorelines[52] and the Earth rotation feedback on sea level[53].

The ice model described above was adjusted to match the newly obtained (RSL) records from the Great Barrier Reef. The analytical uncertainties in RSL were taken into account and the shallow and deep extremes of the RSL envelope were tested. We first employed the ice history model developed by ANU group[4] and ran the GIA model to obtain relative sea level histories for the GBR. The ANU ice model with the same relative ice volumes was then scaled to fit the NOG and HYD RSL. The scaling was done manually within a reasonable range of various parameters and by keeping the relative ice volume of various ice sheets the same as in the original ANU model though keeping the Eurasian ice model almost the same as the ANU model since the history of this ice sheet is reasonably well constrained from both observations and models[54-56] compared to other ice sheets. The chosen Earth parameters (Lithospheric thickness = 70km, Upper mantle viscosity = 2 x 10^{20} Pa s, and Lower mantle viscosity = 10^{22} Pa s) [57,58] fit the GBR region Holocene sea levels well. The analytical uncertainties in RSL and the range in Earth Model parameters (approximately ±2.5 m contribution to GMSL) were used in calculating the MAX and MIN extremes (Extended Data Figs. 8, 9 and Table 4). Supplementary Information shows Global Mean sea level contributions individually for each major ice sheet and for the ANU and highest SL and lowest SL GMSL scenarios (in eustatic terms). The two GMSL curves were then used to construct RSLs in far-field sites with previously published RSL data for comparison (Fig. 4 and Extended Data Fig. 7). Potential Earth model uncertainties were also considered with variable lithosphere thickness and a range of viscosities, of the lower as well as the upper mantle, resulting in more than 60 GIA model experiments. Shaded areas of curves represent possible ranges in RSL for individual sites (Fig. 4 and Extended Data Fig. 7). Visual inspection of the results indicate that the MAX model fits the data remarkably well for almost all the far-field locations tested. In turn, this indicates that the shallow coral habitat depth estimates appear to be sufficiently robust without necessitating extended, deeper water limits.

During the last glacial maximum (30-19 ka; Fig. 3), water depth uncertainties for most samples from the HYD and NOG transects are <5m. Figure 2 shows RSL curves derived from MAX and MIN models. Various Earth rheology parameters were also tested using both MAX and MIN ice models where the shaded region around GMSLs in Extended Data Figure 9 represents the corresponding range in RSLs. During the LGM, the maximum magnitude of RSL difference between the two transects is less than 10 m[59] and hence RSL variations arising from hydro-isostasy are small. The models were run over the maximum possible ranges of the rheological parameters so that the range of RSLs depicted as the shaded zone in Extended Data Fig. 9 cover the full range of possibilities. Traditionally, lower mantle viscosity has been estimated as ca.10^{22} Pa s using far-field RSL observations[57,58], whereas recent studies have reported much higher values of ~7×10^{22} Pa s [4]. Thus, assuming a typical lithospheric thickness and upper mantle viscosity respectively of 70km and 2×10^{20} Pa s, the maximum RSL differences associated with the above range of lower mantle viscosities is ca. 5m (Extended Data Figure 9). This number is smaller than the typical uncertainties inherent in RSL observations at the GBR and, therefore, is well suited for reconstructions of GMSLs during LGM-a and LGM-b. In summary, we concluded that the MAX model provides the best estimate of GMSLs as well as indicating that these tighter depth uncertainties for GBR corals[12] do provide consistent results. Therefore, the extended MIN to MAX range, employed here, well covers the likely range of GMSL constructions with confidence as can be ascertained by visual inspection (Extended Data Figure 9).

Glaciological evidence, including from ice cores cannot easily accommodate the required increase in ice volume. However, the total increase is shared among the large ice sheets (Extended Data Fig. 8). Ice cores retrieved from Antarctica and Greenland are not able to resolve the required magnitude of elevation changes in continental interiors. It is also likely that current ice free regions may have been the places to retain the extra ice at these times. For example, recent evidence suggests that an extensive Ice sheet was grounded on the Ross Sea for at least 3,700 years[60]. New bathymetric data as well as glacial models support these conclusion[61]. However, there is still scope to improve the glaciological models and hence, we hope that our data will contribute to this effort.

Discrepant GMSLs during the LGM at either -120 m or -140 m has been reported respectively for Barbados[7] and the Bonaparte Gulf in North Australia[5]. This has now been reconciled using the recently reported Earth rheology model with J2 observations[10] as well as considering subducting material in Barbados[62]. The model included 65-100km of lithospheric thickness and upper and lower mantle viscosities of $(1–3) \times 10^{20}$ Pa s and 10^{23} Pa s. The global relative sea level observations could reasonably be explained if GMSL during the LGM was ca. -130m. This finding is consistent with the model derived from more than 1,000 far-field RSL observations[4]. The results from the present study, for both the MAX and the MIN options, are respectively -125m and -130m and thus consistent with the independent estimates described above.

Data availability. All the data used in this manuscript is available from Supplementary information of online version of this paper. Modified ANU ice model is available upon reasonable request.

Code availability. Model that we employed in this paper is available from J.O and Y.Y. (yokoyama@aori.u-tokyo.ac.jp) upon reasonable request.

Methods References

31. Camoin, G. F., Seard, C., Deschamps, P., Webster, J.M., Abbey, E., Braga, J.C., Iryu, Y., Durand, N., Bard, E., Hamelin, B., Yokoyama, Y., Thomas, A.L., Henderson, G.M., and Dussouillez, P. Reef response to sea-level and environmental changes during the last deglaciation. IODP Expedition 310 "Tahiti Sea Level". *Geology* **40**, 643-646 (2012).

32. Webster, J. M., Yokoyama, Y., Cotterill, C., and Expedition325Scientist. *Proceedings of the Integrated Ocean Drilling Program 325; Expedition Reports Great Barrier Reef Environmental Changes*. (Integrated Ocean Drilling Program Management International, Inc., 2011).

33. Abbey, E., Webster, J. M., and Beaman, R. J. . Geomorphology of submerged reefs on the shelf edge of the Great Barrier Reef: The influence of oscillating Pleistocene sea-levels. . *Marine Geology* **288**, 61-78 (2011).

34. Bridge, T. C. L., Done, T.J., Beaman, R.J., Friedman, A., Williams, S.B., Pizarro, O., and Webster, J.M. Topography, substratum and benthic macrofaunal relationships on a tropical mesophotic shelf margin, central Great Barrier Reef, Australia. *Coral Reefs* **30**, 143-153 (2011).

35. Yokoyama, Y., Webster, J.M., Cotterill, C., Braga, J.C., Jovane, L., Mills, H., Morgan, S., Suzuki, A. and the IODP 325 Scientists IODP Expedition 325: The Great Barrier Reef Reveals Past Sea-Level, Climate and Environmental Changes since the Last Ice Age. *Scientific Drilling* **12**, 32-45 (2011).

36. Cabioch, G., Montaggioni, L.F., Faure, G., Ribaud-Laurenti, A. Reef coralgal assemblages as recorders of paleobathymetry and sea-level changes in the Indo-Pacific province. Quaternary Science Reviews 18 (14), 1681–1695 (1999).

37. Dechnik, B., Webster, J.M., Webb, G.E., Nothdurft, L., Dutton, A., Braga, J.-C., Zhao, J.-X., Duce, S. and Sadler, J. The evolution of the Great Barrier Reef during the Last Interglacial Period. Global and Planetary Change 149, 53–71 (2017).

38. Yokoyama, Y., Y. Miyairi, H. Matsuzaki and F. Tsunomori Relation between acid dissolution time in the vacuum test tube and time required for graphitization for AMS target preparation, . *Nuclear Instruments and Methods in Physics Research Section B* **259**, 330-334 (2007).

39. Hirabayashi, S., Yokoyama, Y., Suzuki, A., Miyairi, Y. & Aze, T. Multidecadal oceanographic changes in the western Pacific detected through high-resolution bomb-derived radiocarbon measurements on corals. *Geochemistry, Geophysics, Geosystems* **18**, 1608-1617, doi:10.1002/2017gc006854 (2017).

40. Fallon, S. J., Fifield, L. K. & Chappell, J. M. The next chapter in radiocarbon dating at the Australian National University: Status report on the single stage AMS. *Nuclear Instruments and Methods in Physics Research Section B: Beam Interactions with Materials and Atoms* **268**, 898-901, doi:10.1016/j.nimb.2009.10.059 (2010).

41. Druffel, E. R. M. & Griffin, S. Variability of surface ocean radiocarbon and stable isotopes in the southwestern Pacific. *Journal of Geophysical Research: Oceans* **104**, 23607-23613, doi:10.1029/1999jc900212 (1999).

42. Reimer, P. J., Bard, E., Bayliss, A., Beck, J.W., Blackwell, P.G., Bronk Ramsey, C., Buck, C.E., Cheng, H., Edwards, R.L., Friedrich, M., Grootes, P.M., Guilderson, T.P., Haflidason, H., Hajdas, I., Hatté, C., Heaton, T.J., Hoffmann, D.L., Hogg, A.G., Hughen, K.A., Kaiser, K.F., Kromer, B., Manning, S.W., Niu, M., Reimer, R.W., Richards, D.A., Scott, E.M., Southon, J.R., Staff, R.A., Turney, C.S.M., and van der Plicht, J. INTCAL13 and Marine13 radiocarbon age calibration curves 0-50,000 years cal BP. *Radiocarbon* **55**, 1869-1887 (2013).

43. Esat, T. M. Charge collection thermal ion mass spectrometry of thorium. *International Journal of Mass Spectrometry and Ion Processes* **148**, 159-171 (1995).

44. Stirling, C. H., Esat, T. M., Lambeck, K., and McCulloch, M. T. . Timing and duration of the last interglacial; evidence for a restricted interval of widespread coral reef growth. . *Earth and Planetary Science Letters* **160** (1998).

45. Cheng, H., Edwards, R.L., Hoff, J., Gallup, C.D., Richards, D.A., and Asmerom, Y. The half-lives of uranium-234 and thrium-230. *Chemical Geology* **169**, 17-33 (2000).

46. Stirling, C. H., Esat, T.M., McCulloch, M.T., and Lambeck, K. High-precision U-series dating of corals from Western Australia and implications for the timing and duration of the Last Interglacial *Earth and Planetary Science Letters* **135**, 115-130 (1995).

47. Thomas, A. L., G. Henderson, P. Deschamps, Y. Yokoyama, A.J. Mason, E. Bard, B. Hamelin, N. Durand, and G. Camoin. Penultimate Deglacial Sea Level Timing from Uranium/Thorium Dating of Tahitian Corals. *Science* **324**, 1186-1189 (2009).

48. O'Leary, M. J. *et al.* Ice sheet collapse following a prolonged period of stable sea level during the last interglacial. *Nature Geoscience* **6**, 796-800, doi:10.1038/ngeo1890 (2013).

49. Taylor, S. R., and McLennan, S.M. *The continental crust: Its composition and evolution : An examination of the geochemical record preserved in sedimentary rocks.* . (Blackwell Scientific, 1985).

50. Okuno, J., Nakada, M., Ishii, M., and Miura, H. Vertical tectonic crustal movements along the Japanese coastlines inferred from late Quaternary and recent relative sea-level changes. *Quaternary Science Reviews* **91**, 42-61 (2014).

51. Dziewonski, A. M., and Anderson, D.L. Preliminary reference Earth model (PREM). *Physics of the Earth and Planetary Interiors* **25**, 297-356 (1981).

52. Lambeck, K., A. Purcell, P. Johnston, M. Nakada, and Y. Yokoyama. Water-load definition in the glacio-hydro-isostatic sea-level equation. *Quaternary Science Reviews* **22**, 309-318 (2003).

53. Boulton, G. S., P. Dongelmans, M. Punkari, and M. Broadgate. Palaeoglaciology of an ice sheet through a glacial cycle: the European ice sheet through the Weichselian. *Quaternary Science Reviews* **20**, 591-625 (2001).

54. Lambeck, K., C. Smither, and P. Johnston. Sea-level change, glacial rebound and mantle viscosity for northern Europe. *Geophysical Journal International* **134**, 102-144 (1998).

55. Lambeck K, A. Purcell, J. Zhao, N.-O. Svensson. The Scandinavian Ice Sheet: From MIS 4 to the end of the Last Glacial Maximum. *Boreas* **39**, 410–435 (2010).

56. Milne, G. A., and Mitrovica, J.X. Post glacial sea-level change on a rotating earth. *Geophyisical Journal International* **133**, 1-19 (1998).

57. Nakada, M., and Lambeck, K. Late Pleistocene and Holocene sea-level change in the Australian region and mantle rheology. *Geophysical Journal* **96**, 497-517 (1989).

58. Lambeck, K., and Nakada, M. Late Pleistocene and Holocene sea-level change along the Australian coast. *Global and Planetary Change* **89**, 143-176 (1990).

59. Yokoyama, Y., A. Purcell, J.F.Marshall, and K. Lambeck. Sea-leve during the early deglaciation period in the Great Barrier Reef, Australia. *Global and Planetary Change*, **53**, 147-153, (2006).

60. Bart, P., B.J.Krogmeier, M.P.Bart, and S.Tulaczyk. The paradox of a long grounding during West Antarctic Ice Sheet retreat in Ross Sea. *Scientific Reports*, **7**, 1262, doi:10.1038/s41598-017-01329-8, (2017).

61. Halberstadt, A. R. W., Simkins, L. M., Greenwood, S. L. & Anderson, J. B. Past ice-sheet behavious: retreat scenarios and changing controls in the Ross Sea Antarctica. *e Cryosphere* **10**(3), 1003–1020, doi:10.5194/tc-10-1003-2016 (2016).

62. Austermann, J., J.X.Mitrovica, K.Latychev, and G.A.Milne. Barbados-based estimate of ice volume at Last Glacial Maximum affected by subducted plate. *Nature Geoscience*, **6**, 553-557. doi:10.1038/NGEO1859.

63. Edwards, R.L., J.W. Beck, G.S. Burr, D. J. Donahue, J.M.A. Chappell, A. L. Bloom, E.R.M. Druffel, and F.W. Taylor. A large drop in atmospheric $^{14}C/^{12}C$ and reduced melting in the Younger Dryas, documented with ^{230}Th ages of corals. *Science*, **260**, 962-968 (1993).

64. Tarasov, L. and W.R. Peltier. Coevolution of continental ice cover and permafrost extent over the last glacial-interglacial cycle in North America. *Journal of Geophysical Research,* **112**, F02S08 (2007).

Extended Data Legends

Extended Data Figure 1 | Simplified classification of the main coralgal assemblages observed in the Expedition 325 cores. Shallow reef habitats are represented by coral assemblages, cA (massive/robust branching *Isopora* (1) and corymbose *Acropora* gr. *humilis* (2)), cB (branching *Seriatopora* (3), *Acropora* sp. (4)), cC massive/encrusting meruliniids) (5), and cD (encrusting to massive *Porites* (6) and encrusting *Montipora*), when associated with thick crusts of aA1 coralline algae (*Porolithon onkodes*) (7, 8) and vermetid gastropods (8). Deep, fore-reef slope settings are defined by coral assemblages cD (encrusting to massive *Porites* (6) and encrusting *Montipora*, when associated with thin crusts of aA3 (*Mesophyllum* and *Lithothamnion*) (10) and in the absence of aA1 & aA2 (thin *P. onkodes*, *Porolithon gardineri, Harveylithon gr. munitum*) (9).

Extended Data Figure 2|

Representative facies observed in the Expedition 325 cores. The main lithologies are divided into coral reef framework (1-3) and detrital sedimentary facies (4-8).

Extended Data Figure 3 |

Stratigraphic synthesis of inner terrace cores at Mackay. The vertical patterns in coral recovery, lithologies, coralgal assemblages, and vermetid gastropods are summarized here. These data define a major hiatus (red line) in reef development as the top of Reef 2 was exposed following the sea level fall to the LGM-b low-stand (see main text for details). Following deglacial sea level rise, reef growth was re-established as Reef 3b turned on as the shelf is reflooded before this reef drowned after ~14 ka

Extended Data Figure 4 |

Close-up core images showing the boundary between Reef 2 and Reef 3a. Cores M00033A-10R and 11R (HYD-01C) and M00055A-4R (NOG-1B) clearly define the nature of the Reef 2/Reef 3b boundary that represents a major hiatus in reef growth (see Extended Data Figure 3). This boundary is characterized by major changes in lithologies, coralgal assemblages, and diagenetic features, including fresh water, meteoric cements (blue star) indicating the top of Reef 2 has been subaerially exposed.

Extended Data Figure 5 |

Evidence of subaerial exposure. The blocky low magnesium calcite meteoric cement that is related to subaerial exposure is initially precipitated in the intergranular voids of grainstone in 55A 5R1. Then peloids (p) of high magnesium calcite formed under marine condition to fill remaining voids due to submergence following re-flooding. Scale bar in the picture is 100 micrometer.

Extended Data Figure 6 |

Timing and extent of the sea-level drop at LGM-b. Age vs. depth plot showing the key in situ RSL data points from Hydrographer's Passage (HYD-01C) (in blue) and Noggin Pass

(NOG-01B) (in red). AMS-^{14}C-ages derived from corals are indicated by open circles and those derived from coralline algae are indicated by circles with a cross inside. U/Th coral ages are indicated by filled circles. Inflection points defining the maximum position of the RSL at HYD-01C and NOG-01B are also displayed on the figure (see labels NO-5, 8, 9, and HY-3, 5, 6 in Supplementary Information, corresponding respectively to data points 11, 8, 1 and 9, 7, 5 on this figure – see also Fig. 3 in the main text). The combined RSL envelope represented by the black lines (maximum and minimum position) takes into account the uncertainties in the age (2σ), paleowater depth and position in the core of each data point which is illustrated by a colored rectangle (blue for Hydrographer's Passage and red for Noggins Pass) (see Methods for more details). If we were to omit the ^{14}C data due to possible unaccounted variability in local reservoir ages[63], the LGM-b sea level drop defined by coral U/Th ages would be 1.5 ky earlier at 23.5 ka, corresponding to an extended sea level drop over ≈3000 years at ≈7 m/ky. Key RSL index points are: 1. 325-M0053A-13R-1W 21-25 (20.51 ka, 117.93 m; NO-9), 2. 325-M0054B-06R-1W 64-67 (20.50 ka, 124.39 m), 3. 325-M0054B-07R-1W 5-9 (20.47 ka, 125.3 m), 4. 325-M0035A-18R-1W 10-15 (20.43 ka, 127.11 m), 5. 325-M0036A-18R-2W 8-10 (20.70 ka, 128.75 m; HY-6), 6. 325-M0054B-08R-2W 73-75 (22.13 ka, 128.54 m), 7.

325-M0033A-11R-CCW 5-11 (22.11 ka, 106.83 m; HY-5), 8. 325-M0055A-04R-1W 35-40b (21.87 ka, 103.13 m; NO-8), 9. 325-M0032A-10R-1W 18-20 (23.49 ka, 107.95 m, HY-3), 10. 325-M0033A-13R-CCW 1-3 (23.62 ka, 109.46 m), 11. 325-M0055A-04R-2W 99-105 (23.97 ka, 104.84 m; NO-5).

Extended Data Figure 7 |

GIA results for selected sites. Calculations, for selected far-field sites (a-f), using the ice model based on the lower-bound of RSL from GBR. GIA calculations implemented using parameters of upper mantle viscosity and lithospheric thickness10^{20} Pa s and 70 km and lower mantle viscosity of 10^{22} Pa s. However, the differences between data and calculations for far-field sites of Tahiti (b), Bonaparte (c) and Sunda(d) indicate a better match with GIA when the higher RSL obtained from this study is used (Fig 4) in calculating the global deglacial sea levels. The grey band represents the range of RSL predictions using GIA modelling with various earth parameters (Lithospheric thickness H = 70km, Upper mantle viscosity = 10^{20}-10^{21} Pa s, Lower mantle viscosity = 10^{21} -10^{23} Pa s), and a melting model (ie., ice history) which, in this case, was the MIN model. The red lines are for Lithospheric thickness H= 70km, upper mantle viscosity = $2x10^{20}$ Pa s, lower mantle viscosity = 10^{22} Pa s. The blue lines show the case for lithospheric thickness H=70km, upper mantle viscosity = $2x10^{20}$ Pa s, lower mantle viscosity = 10^{23} Pa s.

Extended Data Figure 8 |

Comparisons between ANU GMSL and the present new GBR based GMSL. The blue curves represent the ANU GMSL results[4] whereas the red bands, covering a range of GBR RSL based GMSL, are from our study. During the transition from LGM-a to LGM-b, around 21 ka, there is enhanced precipitation over the North American Ice Sheet and to a lesser extent over Antarctica, although, for the latter, the ice volume continues to build up, for longer, until the termination of LGM-b at ca.17 ka. The manually adjusted nominal ANU ice model will influence our inferred melting history for each ice sheet. Furthermore, although, the ANU model differs in some respects from other ice sheet reconstructions, eg., (ref. 64) the results from these simulations are not significantly different.

Extended Data Figure 9 |

GIA model results for HYD and NOG with different viscosity settings. MAX (a) and MIN (b) represent the maximum and minimum extremes of GBR RSL. Blue and red bands are relative sea level ranges derived from our study for Hydrographyer's passage (HYD) and Noggin Pass

(NOG). Gray bands represent the range of predicted sea levels using the new ice model. Lithospheric thickness is fixed at 70 km, whereas mantle viscosities for upper and lower mantle varied between 10^{20}-10^{21} Pa s and 10^{21}-10^{23} Pa s. RSL predictions for representative viscosities for HYD-01C and NOG-01B are shown as red and blue solid and dotted lines respectively. V_{up} and V_{low} represent the upper and lower mantle viscosity values (side panel).

Extended Data Table 1 |

Simplified coral and coralline algal assemblages and their likely paleoenvironmental setting.

*When associated with centimetre-scale thick aA1 CAR crusts and vermetid gastropods.□**When associated with thin crusts of aA3 and lacking vermetid gastropods.□***Paleowater depths were estimated by comparison with their modern Indo Pacific counter parts.

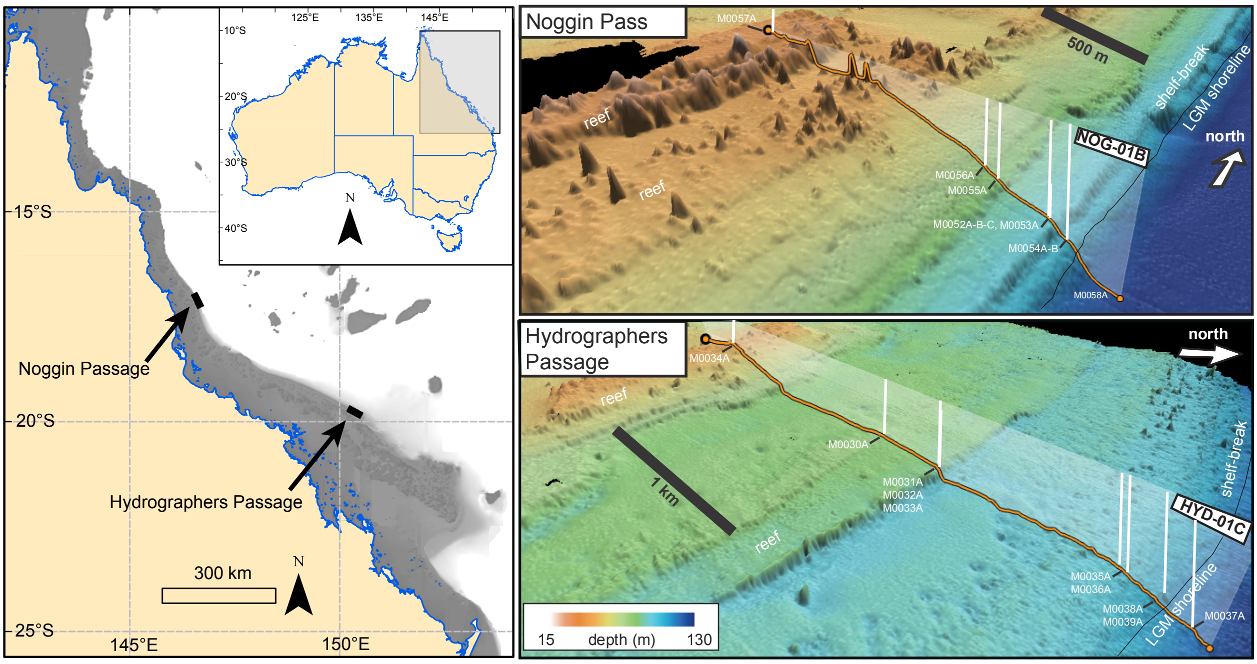

125°E
135°E
145°E
10°S
20°S
30°S
40°S
N
15°S
Noggin Passage
20°S
Hydrographers Passage
300 km
N
25°S
145°E
150°E
Noggin Pass
M0057A
500 m
reef
reef
shelf-break
LGM shoreline
NOG-01B
north
M0056A
M0055A
M0052A-B-C, M0053A
M0054A-B
M0058A
Hydrographers
Passage
north
M0034A
reef
M0030A
1 km
M0031A
M0032A
M0033A
reef
shelf-break
HYD-01C
M0035A
M0036A
M0038A
M0039A
LGM shoreline
M0037A
15
depth (m)
130

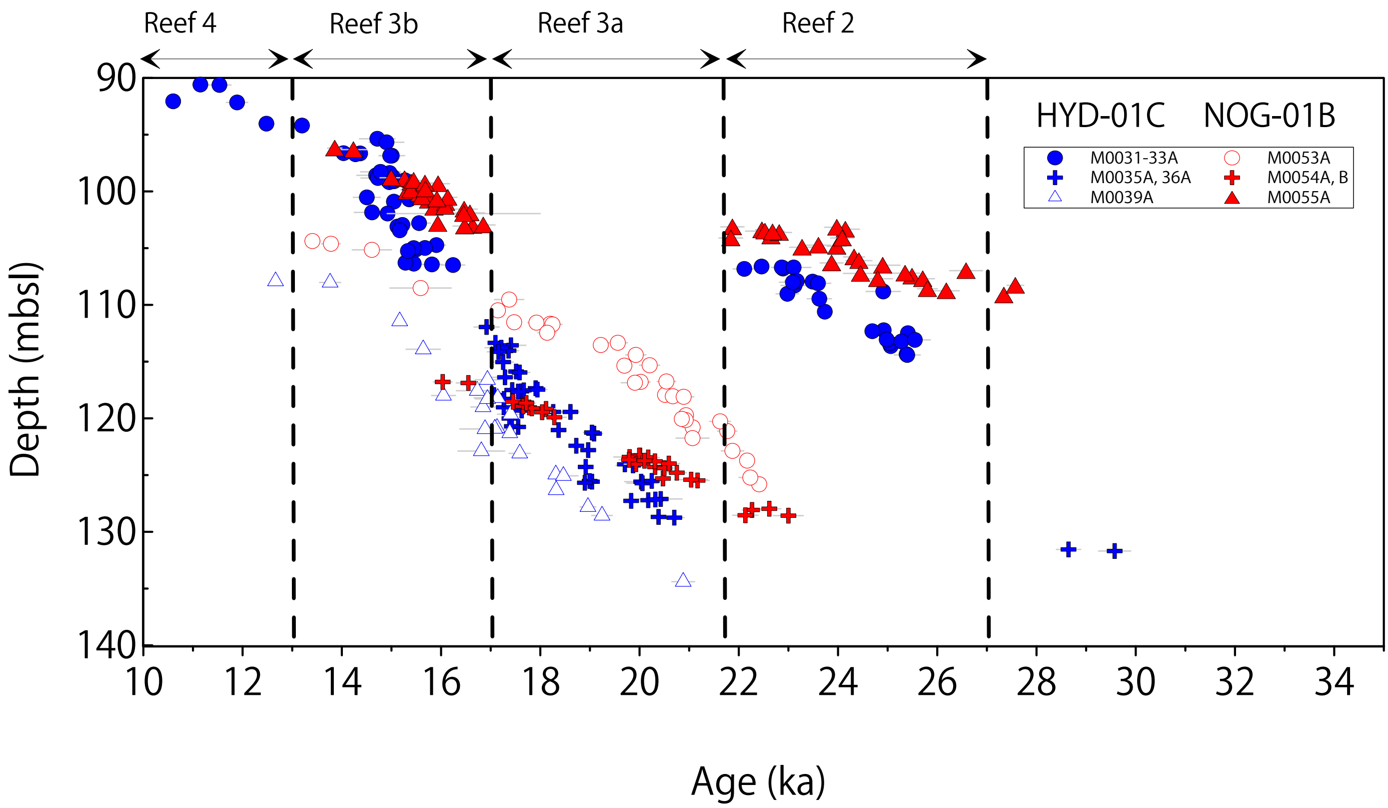

Yokoyama et al. (Fig2)

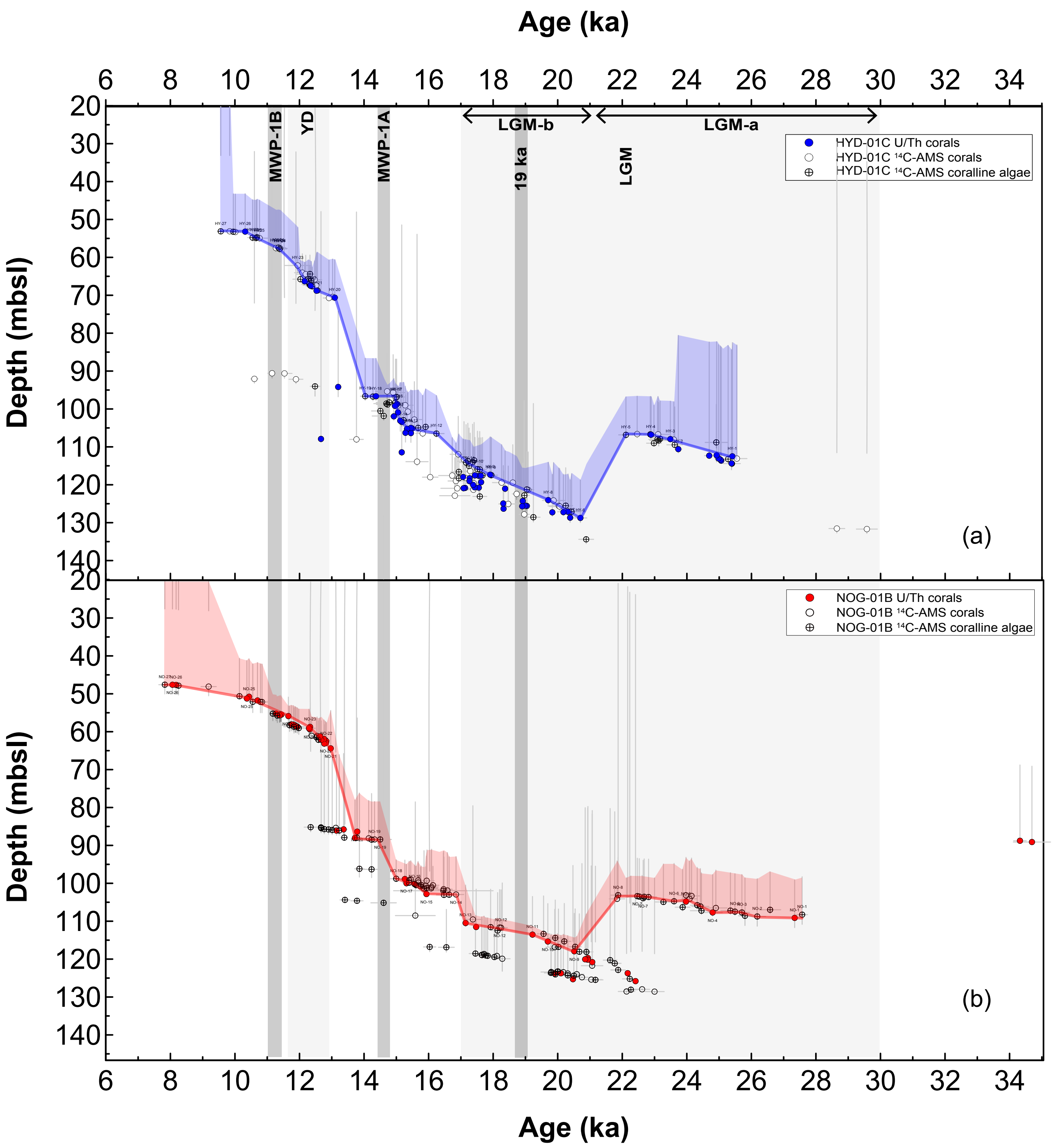

Yokoyama et al. (Fig3)

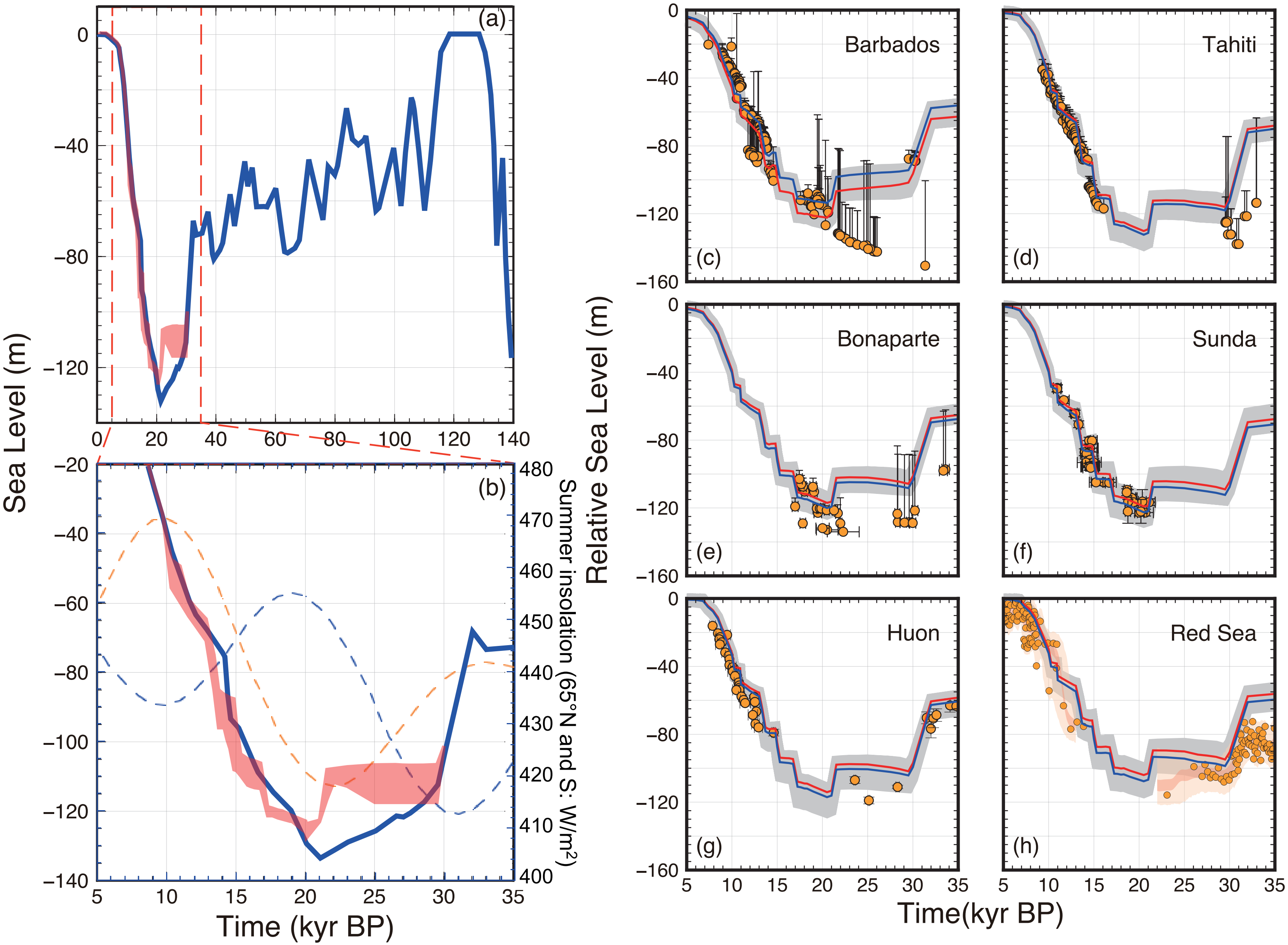

Yokoyama et al. (Fig 4)